Isman Khazi*, Andras Kovacs, Vaibhav Kumar, Pranav Dhumal, Ulrich Mescheder
Institute of Microsystems Technology, Faculty of Mechanical and Medical Engineering, Furtwangen University

Microfabricated 2D planar eddy-current microcoils for the non-destructive testing of grinding burn marks

Mikrofabrykowane płaskie wiroprądowe mikrocewki 2D do nieniszczących badań błędów szlifierskich

ABSTRACT

Microtechnology based 2D planar eddy-current microcoils (μCoils) are simulated and fabricated for the detection of grinding burn marks in conductive materials such as industrial hard steels, which are predominantly used for manufacturing of structured parts using grinding. COMSOL multiphysics simulation tool is used to simulate μCoils with various geometries, namely: circular spiral, circular non-spiral and meander type geometry, to investigate the influence of the frequency on the resultant impedance of the μCoil as a function of the grinding burn marks. The simulation results show that the impedance of the μCoil of all geometries varies in response to a 1500 μm wide grinding burn mark. The sensitivity of the μCoil to detect even grinding burn marks with 200 μm width is improved by modifying the wire width of the non-spiral μCoils. Furthermore, as a proof of concept non-spiral μCoils with varying number of turns (5,10 and 20) were fabricated using ferromagnetic nickel-cobalt alloys. The experimental results show that the impedance of the fabricated μCoils varies as a function of the grinding burn mark present on a 42CrMo4 workpiece.

Keywords: *2D planar coils; grinding burn marks; non-destructive testing (NDT) and micro eddy-current sensor*

STRESZCZENIE

Płaskie wiroprądowe mikrocewki 2D (μCoils) oparte na mikrotechnologii przebadano numerycznie a następnie wytwarzano w celu wykrywania śladów lokalnego przegrzania w materiałach przewodzących, takich jak przemysłowe stale twarde, które są głównie wykorzystywane do produkcji elementów konstrukcyjnych przy użyciu technologii szlifierskich. Oprogramowanie do numerycznych obliczeń wielofizycznych COMSOL zostało użyte do symulacji mikrocewek μCoil o różnych geometriach w celu zbadania wpływu częstotliwości na wynikową impedancję μCoil w funkcji szlifowania śladów przegrzania. Wyniki symulacji pokazują, że impedancja μCoil we wszystkich geometriach zmienia się pod wpływem śladu po szlifowaniu o szerokości 1500 μm. Wrażliwość μCoil na wykrywanie śladów przegrzania nawet o szerokości 200 μm jest poprawiona poprzez modyfikację szerokości drutu nie spiralnych mikrocewek. Ponadto, jako dowód słuszności koncepcji, wykonano niespiralne cewki o zmiennej liczbie zwojów (5,10 i 20) przy użyciu ferromagnetycznych stopów nikiel-kobalt. Wyniki eksperymentów pokazują, że impedancja wytworzonych mikrocewek zmienia się w zależności od śladu po szlifowaniu obecnego na elemencie wykonanym z 42CrMo4.

Słowa kluczowe: *cewki płaskie 2D; szlifowanie śladów przegrzań; badania nieniszczące (NDT) i mikro przetwornik wiroprądowy*

1. Introduction

The use of eddy-current technique is well-established as electromagnetic sensing method for the non-destructive testing (NDT) with excellent knowledge base and sophisticated test systems for the detection of material flaws such as cracks, pores, material structural changes etc. [1]. However, the conventional sensors (i.e. the wire wound eddy-current probes) are limited in their capability for the detection of small size workpieces (for e.g. miniaturized ball bearings etc.) and material defects in micrometer dimensions in the workpiece [2]. The feasibility of using planar eddy-current microcoils (μCoils) fabricated using microtechnology for NDT of material flaws in the micrometer range, such as microcracks and micro-pores, has been reported by several research groups in the last two decades [3–5]. The significant advantage of using μCoils over conventional wire wound eddy-current probes is not only their higher sensitivity to detect material defects even in micrometer dimensions, but also their small size, which makes them capable of testing miniatured workpieces [2,6]. Additionally, considering the current trend towards industry 4.0, the in-situ detection of material flaws during the material structuring can also be achieved by integration of miniaturized eddy-current μCoils in the vicinity of the material processing tools for real-time smart process monitoring.

Apart from conventional existing material flaws such as cracks, holes etc., the prevalence of grinding burn marks has been of concern recently as a detrimental material flaw for the quality of the workpiece, which is fabricated using grinding [7,8]. The grinding burn marks are caused by excessive thermal energy, resulting in the local modification of the boundary region in the workpiece and thus changing the material structure and inducing localized residual stresses [7,9]. Therefore, an early detection of the grinding burn marks during the grinding process (which can facilitate in optimization of grinding parameters) and post fabrication testing, is of enormous importance in order to maintain the quality of the workpiece. The grinding burn marks can be detected with destructive or expensive methods such as Nitol etching or x-ray diffraction (XRD) [7]. Furthermore,

*Corresponding Author. E-mail: kmi@hs-furtwangen.de

Published by „Badania Nieniszczące i Diagnostyka" SIMP Publishing Agenda
DOI: 10.26357/BNiD.2019.012

recently NDT electromagnetic sensing methods such as Barkhausen noise methods and eddy current sensors have also been reported to be suitable for their detection [3-4]. However, the use of μCoils for the detection of the grinding burn marks is not yet reported. Therefore, the feasibility of using μCoils for the detection of grinding burn marks is shown in this work with the help of finite element method simulation of μCoils and as proof of the concept preliminary experimental results are reported.

2. Concept of eddy-current testing using absolute probe

NDT using eddy-current technique works on the principle of electromagnetic induction, wherein the μCoil is driven by an alternating current of a certain frequency, which results in the formation of an alternating magnetic field around the μCoil, called as the primary magnetic field. When a conducting workpiece is approaching the μCoil, the alternating magnetic field results in swirling currents in the workpiece, referred to as the eddy-currents. The induced eddy-current produces their own magnetic field, which is referred as secondary magnetic field, which in turn opposes the primary magnetic field according to the Lenz's law. The presence of any material flaw on the workpiece, effects the nature in which the eddy-currents are induced. Consecutively, the primary magnetic field and the resultant impedance of the μCoil are affected, thereby, facilitating the detection of the material flaws. The impedance (Z) of coil predominantly consists of the coil resistance (R) and inductance reactance (X_L), which is the function of the inductance of the coil (L) and the frequency (f) as shown in equation 1. Furthermore, the capacitive reactance for an inductive coil is usually neglected. The resultant absolute impedance of a coil is the vector sum of the resistive part and the inductance reactance as shown in equation 2.

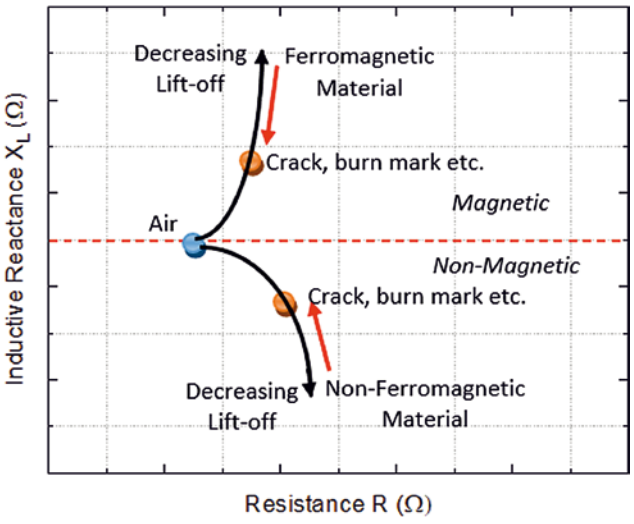

Fig. 1. Schematic impedance plot trajectory of an absolute eddy-current sensor for a ferromagnetic and non-ferromagnetic material.

Rys. 1. Schemat trajektorii impedancji czujnika wiroprądowego w konfiguracji absolutnej dla materiału ferromagnetycznego i nieferromagnetycznego.

$$X_L = 2\pi f L \quad (1)$$

$$Z = \sqrt{R^2 + X_L^2} \quad (2)$$

Furthermore, the impedance change in response to the conductive workpiece is different for ferromagnetic and non-ferromagnetic material as shown in impedance trajectory plot in Figure 1. The distance between the μCoil and the workpiece, which is called "lift-off" is critical for the operation of the sensor. As the sensor μCoil is brought in the proximity of a non-ferromagnetic workpiece such as aluminum, copper etc., the induced eddy-currents adversely affects the primary magnetic field of the μCoil thereby, decreasing the inductance reactance of the coil and the energy used for inducing eddy-current, which is dissipated as heat, resulting in increasing the resistive part of the μCoil. Besides, when a ferromagnetic material such as steel is brought in proximity of the sensor μCoil, the primary magnetic field of the μCoil is amplified owing to the high permeability of the ferromagnetic workpiece. Consecutively, the inductive reactance of the μCoil is increasing along with resistive part. However, the inductive reactance increase is predominant in case of ferromagnetic workpiece. In presence of a material flaw such as grinding burn mark, the conductivity in case of the non-ferromagnetic material and the permeability in case of ferromagnetic material is affected. Consecutively, the nature of the induced eddy-current changes; thereby, affecting the resultant impedance of the μCoil. In principle, the impedance of the μCoil increases to Z_{wp} from its primary value Z_{air} (i,e. when the sensor μCoil is in air) in presence of a conductive workpiece and it reduces to Z_{bm} in presence of any material flaws. The eddy-current probes can be used in various configurations. When a single μCoil is used, then it is referred to as an absolute sensor, wherein the impedance of the μCoil is affected by the presence of the material flaws in the workpiece. Furthermore, when two μCoils are used (operates based on transformation principle), wherein one μCoil serves as sending coil (which is driven by AC current) and the other serves as the receiver coil. The voltage of the receiver coil changes as a function of material flaw and hence serves as the detection signal. However, from the microfabrication point of view, an absolute sensor can be fabricated with ease as it involves less fabrication steps, therefore an absolute sensor is considered in this work.

3. Simulation of MEMS eddy-current μCoils

3.1 Simulation construction and definition of the grinding burn marks

μCoils can be of various geometries for rectangular spiral type, circular spiral type, non-spiral type, meander type, etc. However, each one of them have their own advantages and disadvantages. Furthermore, to use a μCoil as eddy-current probe, it should have ideally high inductance (L) value (to produce stronger magnetic field) and low resistance (R) to avoid ohmic losses. High L can be obtained by decreasing the distance between the individual wires and increasing the number of turns (which adversely affect R) in the μCoil and R can be reduced by increasing the thickness of the

individual wires in the µCoil. The impedance characteristics of the absolute µCoils are simulated using COMSOL Multiphysics software with AC/DC module. Circular spiral type, circular non-spiral type and meander type µCoil geometries are simulated for the detection of the grinding burn marks.

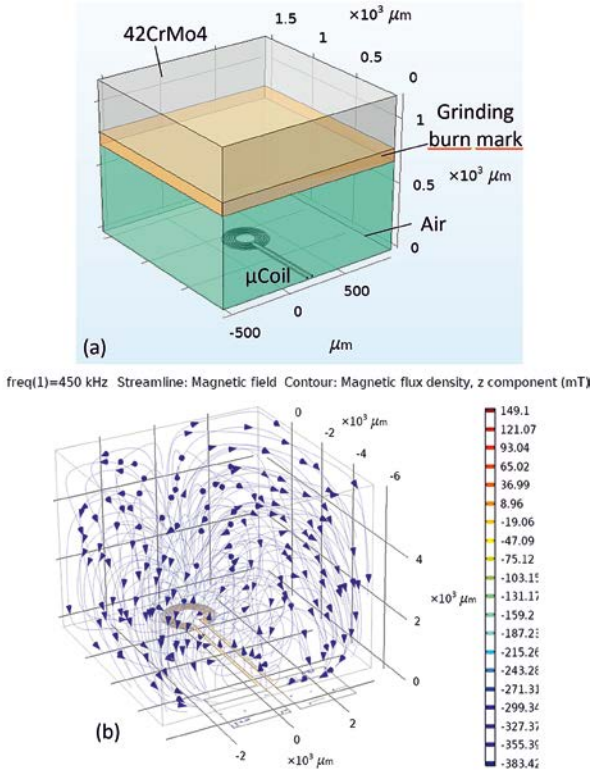

Fig. 2. (a) 3D simulation setup consisting of µCoil, grinding burn mark (depth 100 µm) and 42CrMo4 workpiece, (b) simulated magnetic field of the non-spiral µCoil at 450 kHz

Rys. 2. (a) Konfiguracja modelu symulacji 3D składająca się z µCoil, śladu przegrzania po szlifowaniu (głęb. 100 µm) i badanego elementu wykonanego z 42CrMo4, (b) obliczony przebieg pola magnetycznego dla cewki niespiralnej przy częstotliwości 450 kHz.

On contrary to microcracks, which can be defined as air spaces in workpiece for simulation purpose, the definition of grinding burn mark is more challenging, as there are no defined norms for the grinding burn marks. They occur in the workpiece due to excessive localized heating and sudden cooling with lubricants during the grinding process, thereby, resulting in thermal damage in the boundary layer with complex material changes involving changes in hardness, residual stress, conductivity (σ) and relative permeability (µr). For the simulations, low alloyed high-grade chrome-molybdenum ferritic steel, i.e. 42CrMo4, is considered as the workpiece, which is one of the common materials used for grinding processes. In the simulation, the grinding burn marks can be defined as the change in µr and σ of the workpiece. Considering the ferromagnetic nature of the selected workpiece 42CrMo4, the change in µr is considered predominant (as described in section 2) and therefore, used as material parameter for the definition of the grinding burn mark. A 3D simulation setup consisting of the µCoil, grinding burn mark and the workpiece is constructed as shown in Figure 2 (a). The distance between the µCoil and workpiece (42CrMo4: 1500µm², height 500 µm) is set to 700 µm for all the simulations, a value used typically in conventional eddy-current set-ups. Figure 2 (b) shows the primary magnetic field produced by circular non-spiral coil (5 turns, copper wire with width, thickness and distance between the wires all chosen as 20 µm) in response to 80 mA alternating current at 450 kHz frequency.

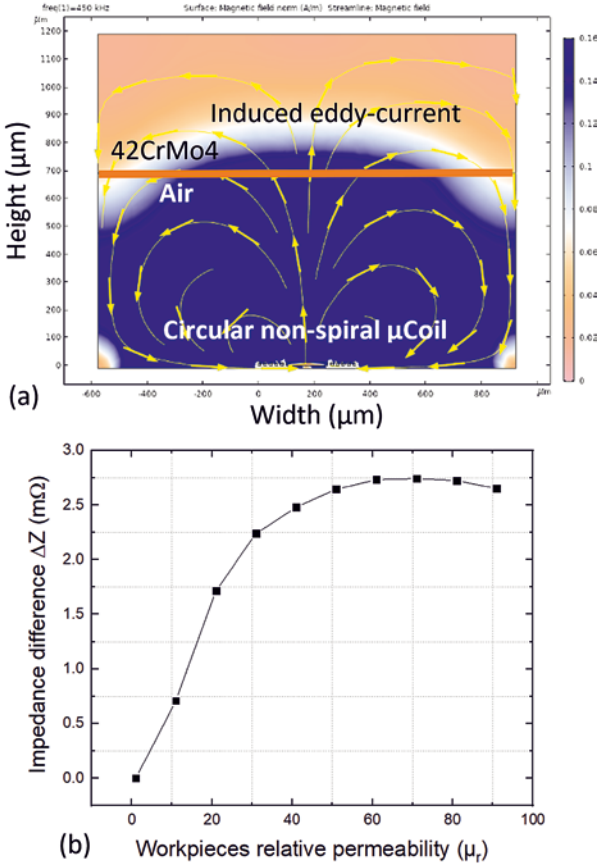

Fig. 3. (a) Simulated induced eddy-current in the workpiece without grinding burn mark in response to the primary magnetic field of the circular non-spiral µCoil at 450 kHz, 80 mA. (b) Simulated normalized impedance of the µCoil as changing relative permeability of the workpiece (42CrMo4).

Rys. 3. (a) Obliczony prąd wirowy zaindukowany w elemencie obrabianym nieposiadającym śladu przegrzania szlifierskiego w odpowiedzi na pierwotne pole magnetyczne okrągłej nie spiralnej cewki przy 450 kHz, 80 mA. (b) Obliczona znormalizowana impedancja cewki µCoil jako zmieniająca się względna przenikalność przedmiotu badanego (42CrMo4).

3.2 Simulation results

In order to test the sensitivity of the µCoil to varying relative permeability, the impedance response of the µCoil to variable µr (0-1000) of the workpiece without grinding burn mark is initially simulated. Figure 3(a) shows the induced eddy-current in the workpiece (42CrMo4) in response to the alternating primary magnetic field of the circular non-spiral µCoil driven at 80 mA and 450 kHz frequency. Figure 3(b) shows the impedance difference of the µCoil as a function of varying µr of the workpiece. As discussed in section 2, the inductive reactance predominantly increases for ferromagnetic

materials and with higher μr the primary magnetic field is further amplified (similar effect as resulted by magnetic core), thereby, increasing Z of the μCoil as shown in Figure 3(b). However, with μr>60 the affect gradually saturates and consecutively the change in Z also saturates. The grinding burn mark of 100 μm thickness is defined on the workpiece as shown in Figure 2(a) and the width of it is varied in two extremities namely: 200x1500 μm and 1500x1500 μm. The material property that differentiates the grinding burn mark from the workpiece is μr, it is defined for the starting conditions as 20 and 28 for the grinding burn mark and the workpiece, respectively. Three different μCoil geometries, chosen in respect to fabrication issues namely: circular non-spiral, circular spiral and meander type geometries are simulated as shown in Figure 4(a-c), respectively. Wherein, the geometry in Figure (a) and (c) can be realized by one layer microfabrication whereas type (b) needs to layers and thus is more complex to realize by planar microfabrication. For the simulation, the μCoils wires are defined as copper with a width, height and inter-wire distance of each 20 μm, respectively. A constant area of 0.125 mm² is used for the μCoil of all the geometries.

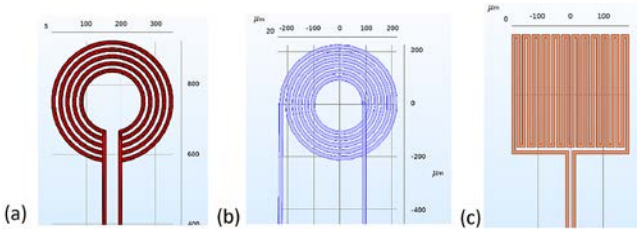

Fig. 4. μCoil geometries selected for the simulation (a) circular non-spiral μCoil, (b) circular spiral μCoil and (c) meander type μCoil.
Rys. 4. Geometria cewki μCoil wykorzystana w trakcie symulacji (a) okrągła niespiralna μCoil, (b) spirala okrągła cewka μCoil i (c) meandralna cewka μCoil.

Figure 5 (a) shows the impedance response of the μCoil (non-spiral circular) in air for a parametric frequency sweep between 100 kHz-500 kHz, wherein Z increases as function of frequency (as shown in equation 1). The frequency range was selected considering the fact that the grinding burn marks are more superficial when compared to other material flaws and the eddy-current depth penetration (δ) is inversely proportional to frequency as shown in equation

$$\delta = \frac{1}{\sqrt{\pi f \sigma \mu_r}} \tag{3}$$

The change in impedance for non-spiral 5 turns μCoil is negligible for the grinding burn mark of 200 μm width and increases for the 1500 μm wide grinding burn mark as shown in Figure 5(b) and specifically for 450 kHz frequency as a function of measurement condition in Figure 5(c). In the presence of the workpiece, the impedance of the μCoil increases from Zair to Zwp owing to induced eddy-currents. Furthermore, in presence of grinding burn marks the nature of the induced eddy-current is affected by the lower μr of the grinding burn marks, thereby, reducing the impedance from Zwp to Zbm. Moreover, f range used in the simulation of the μCoil does not influence significantly the Z of μCoil as a function of grinding burn mark as shown in Figure 5(b). The Z response of the meander type and of the spiral μCoil to the presence of grinding burn mark is shown in Figure 6(a) and (b), respectively. Figure 6(c) shows the Z response of spiral μCoil at 450 kHz, which shows the Z shift in relation to the measurement condition. Furthermore, the circular non-spiral μCoil was modified by increasing the wire width (w) using the equation (4), where n is the number of individual wires from the innermost circle of μCoil. The inter-wire distance and thickness of wire was similar as the previous μCoils and the resultant μCoil geometry is shown in Figure 7(a) and its impedance response is shown in Figure 7(b).

$$w = n \times 25\ \mu m \tag{4}$$

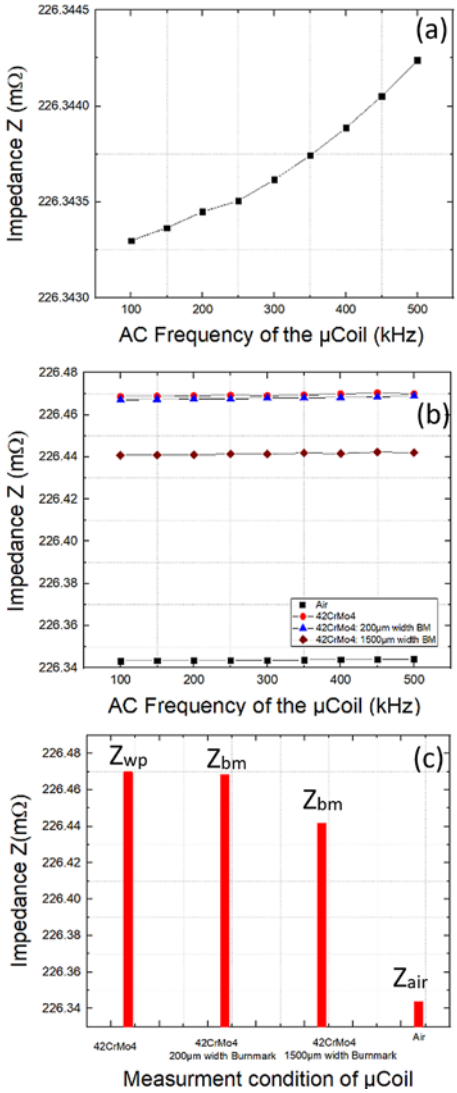

Fig. 5. Simulated Z response of the circular non-spiral μCoil (a) μCoil in air as a function of frequency, (b) as a function of grinding burn mark (200 μm width and 1500 μm width) and (c) as a function of μCoil measurement condition at 450 kHz.
Rys. 5. Symulowana odpowiedź impedancji Z okrągłej niespiralnej cewki μCoil (a) dla μCoil w powietrzu w funkcji częstotliwości, (b) wyrażona jako funkcja śladu szlifowania (szerokość 200 μm i szerokość 1500 μm) oraz (c) wyrażona jako funkcja warunków pomiaru μCoil przy 450 kHz.

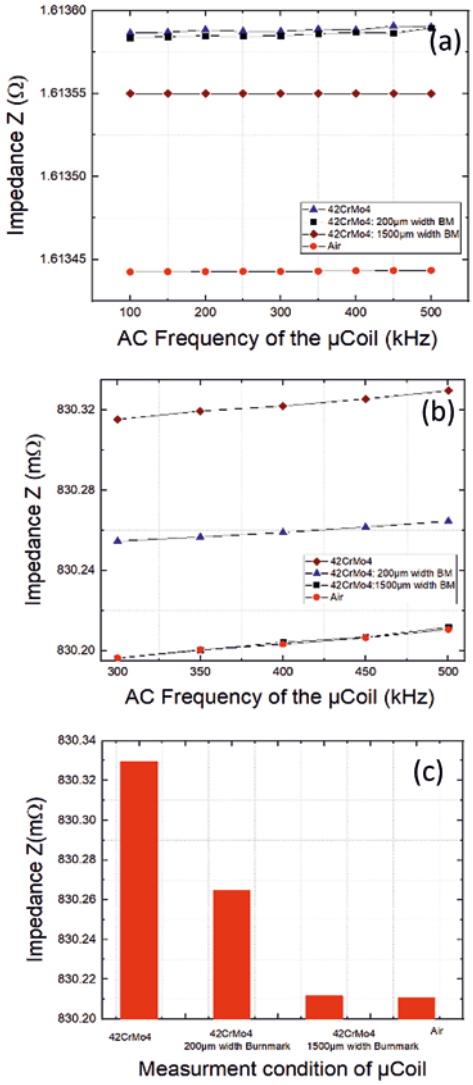

Fig. 6. Simulated Z response of the µCoil for (a) meander type µCoil, (b) circular spiral µCoil and (c) as a function of circular spiral µCoil measurement condition at 450 kHz.

Rys. 6. Symulowana odpowiedź impedancji Z µCoil dla (a) meandralnej cewki, (b) spiralnej cylindrycznej cewki µCoil i (c) w funkcji warunków pomiaru spiralnej cylindrycznej cewki przy częstotliwości 450 kHz.

The magnitude of impedance change (i.e. $\Delta Z=Z_{wp}-Z_{bm}$) depends on the intensity of the grinding burn mark and its dimensions. The ΔZ values for all the 4 different simulated µCoil geometries are shown in Figure 7(c) as a function of width of the grinding burn mark. The ΔZ value of non-spiral and meander type coil is smallest and almost similar, among all geometries. They could not detect the grinding burn mark with 200 µm width. The largest ΔZ value is obtained for the modified non-spiral µCoil for both 200 µm width and 1500 µm width grinding burn mark as shown in Figure 7(c). This can be attributed to the increased magnetic field strength produced by the modified geometry of the µCoil, which resulted in a more pronounced induction of eddy-currents in the workpiece. Also, the spiral µCoil can detect both, small and large width grinding burn marks. However, from the microfabrication point of view it is complex as it requires the bridge connection from the innermost wire to the contact pad. Therefore, the modified non-spiral µCoil provides a better geometrical design for microfabrication.

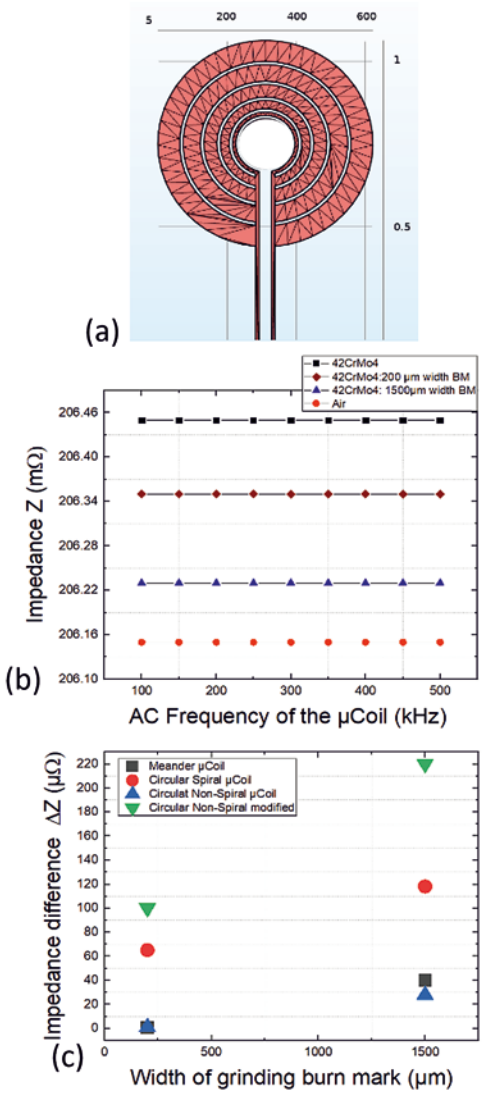

Fig. 7. (a) Modified circular non-spiral µCoil with varying wire width (red) as defined in eq. (4), (b) impedance response of modified non-spiral µCoil as function of grinding burn mark and (c) comparison of the impedance difference (ΔZ) for the varying geometries of µCoils at 450 kHz.

Rys. 7. (a) Zmodyfikowana cylindryczna niespiralna cewka µCoil o zmiennej szerokości drutu (czerwony kolor) zgodnie z definicją w równaniu. (4), (b) odpowiedź impedancyjna zmodyfikowanego niespiralnej cewki wyrażona jako funkcja śladu szlifowania oraz (c) porównanie różnicy impedancji (ΔZ) dla różnych geometrii cewki przy częstotliwości 450 kHz.

4. Experimental results

4.1 Microfabrication of eddy-current µCoils

For the proof of concept µCoils were fabricated using ferromagnetic nickle-cobalt alloys, however, copper µCoil will also be fabricated for future work. The microfabrication of the µCoils was done on 4 inch (100) monocrystalline silicon wafers sputter coated with titanium (Ti) and platinum (Pt) 20 nm and 100 nm thick, respectively. The Ti layer was used as the adhesion promoter for the Pt plating base. AZ4652 positive photoresist was spin coated on the wafer at 700 rpm

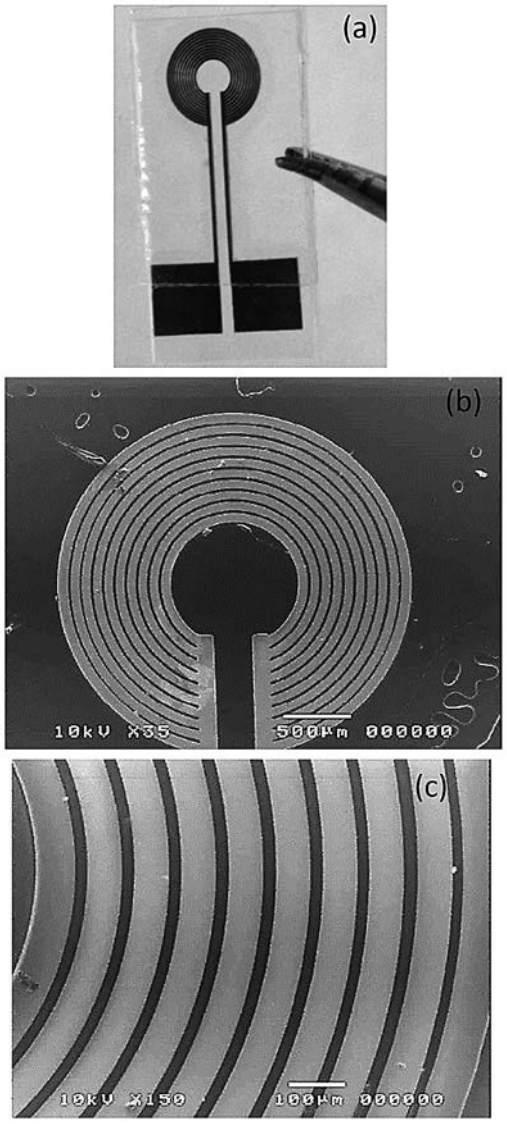

Fig. 8. Fabricated circular non-spiral µCoils using ferromagnetic nickel-cobalt alloy with 10 turns with wire width 50µm, thickness 20µm and inter-wire distance 20µm (a) µCoil on a glass chip, (b) SEM micrograph of 10 turns µCoil and (c) magnified SEM micrograph.

Rys. 8. Wytworzone okrągłe niespiralne cewki µCoil przy użyciu ferromagnetycznego stopu niklowo-kobaltowego z 10 zwojami o szerokości drutu 50 µm, grubości 20 µm i odległością między drutami 20 µm (a) cewka µCoil na chipie szklanym, (b) mikrografia SEM 10 zwojów µCoil i (c) powiększony mikrograf SEM.

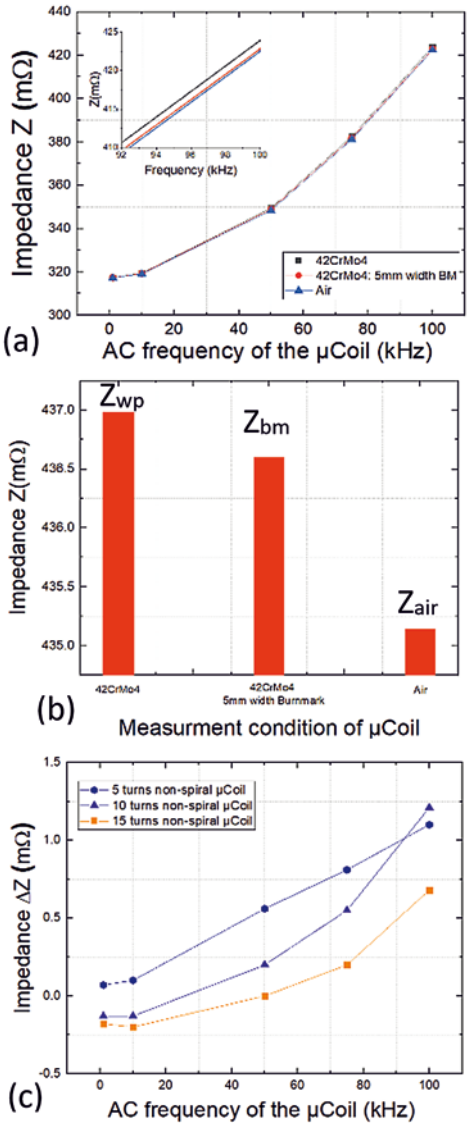

Fig. 9. Experimental characterization of non-spiral µCoil for the detection of 5mm width grinding burn marks on 42CrMo4 workpiece, (a) Z response of 5 turn µCoil as a function of frequency, inset: Z in the linear range around 100 kHz,(b) Z response of 5 turn µCoil at 100 kHz and (c) ΔZ of non-spiral µCoil with 5, 10 and 20 turns for 5 mm grinding burn mark.

Rys. 9. Eksperymentalna charakterystyka niespiralnej cewki µCoil do wykrywania śladów po szlifowaniu o szerokości 5 mm na elemencie 42CrMo4, (a) Odpowiedź impedancji Z dla 5 zwojów cewki µCoil w funkcji częstotliwości, rysunek wewnątrz: Z w zakresie liniowym w okolicy 100 kHz, (b) odpowiedź Z dla 5 zwojów cewki µCoil przy 100 kHz oraz (c) ΔZ niespiralnej cewki µCoil z 5, 10 i 20 zwojami dla 5 mm śladu szlifierskiego.

Tab. 1. Electrolyte constituents for the electrodeposition of µCoils using ferromagnetic nickel-cobalt alloys.

Tab. 1. Składniki elektrolitu do elektroosadzania cewek µCoil przy wykorzystaniu ferromagnetycznych stopów niklowo-kobaltowych.

Eelctrotyle constituent	Concentration
$Ni(NH_2SO_3)2 \cdot 6H_2O$	1.8 mol/l
$Co(NH_2SO_3)2 \cdot 6H_2O$	0.03 mol/l
H_3BO_3	0.5 mol/l
Deionized H_2O	14 mol/l
Bath pH value	4.5
Temperature	45°±2°C

spin speed, 2000 rpm/sec acceleration for 30 seconds to get a 20 µm photoresist thickness, which was followed by a prebake step on hotplate at 100°C for 50 seconds. The circular non-spiral µCoil geometry with 5, 10 and 20 turns with wire width = 50 µm and inter-wire distance = 20 µm was exposed on the wafer coated with photoresist using Karl Suss MA6 mask aligner with using mercury lamp with I-line wavelength of 365.4 nm for 90 seconds. Post exposure, the photoresist was developed in the solution containing deionized water and AZ315B in 4:1 ratio for 6 minutes, which was followed by post bake step on hotplate at 115°C for 50

seconds. Before the electrodeposition process, the wafer was dipped in buffered hydrofluoric acid for 30 seconds to activate the surface. The electrodeposition was carried in the sulfamate bath (the electrolyte composition is shown in Table I) containing nickel and cobalt ions at 5 mA/cm² for 40 minutes to get 20 µm thick µCoils with an alloy containing 30wt% cobalt. Post electrodeposition the µCoils were transferred from the silicon wafer to a glass chips (5 x 10 mm) and were held on it by polymer adhesive film for the characterization of the µCoils as shown in Figure 8(a). The micrographs of the µCoils taken by scanning electron microscope (SEM) are shown in Figure 8(b-c) for 10 turn non-spiral µCoil.

4.2 Characterization of the µCoils

The contact pads of the µCoil were soldered with 400 µm diameter zinc coated copper wires to connect the µCoils with a Hioki 3522-50 LCR meter (limited to frequencies up to 100 kHz). The impedance and inductance of the µCoils as a function of the grinding burn marks was recorded. 42CrMo4 was used as the workpiece which had 5mm width grinding burn marks on it. The impedance of the µCoil was recorded at frequencies of 1, 10, 50, 75 and 100 kHz in three measurement conditions, namely: in air and on 42CrMo4 with and without burn mark. A constant lift-off of 500 µm defined by the thickness of the glass chip on which the µCoil was held as shown in Figure 8(a). This value is close to the 700 µm chosen for simulation. Similar to the simulation results, the Z value of the µCoil increases in presence of a conductive material in its proximity and then decreases in response to material flaws such as grinding burn marks in this case as shown in Figure 9(a-b) for 5 turn µCoil at 100 kHz. The ΔZ of the µCoil with 5, 10 and 20 turns is shown in Figure 9(c), wherein, on one hand the signal strength i.e. ΔZ increases as a function of coil frequency. While, on the other hand the ΔZ value decreases as the µCoils number of turns increases, which can be attributed to the stronger magnetic field created, which are then amplified by ferromagnetic 42CrMo4, which partly dominates the effect of the grinding burn mark. In comparison to the simulation results, the ΔZ value in case of the fabricated µCoils is higher, which can be attributed to the 50 µm width of the wire, the ferromagnetic nickel-cobalt alloys use for the fabrication of the µCoils and the wider grinding burn mark with a width of 5 mm.

5. Discussion and conclusion

Microfabricated planar µCoils with different geometries as absolute eddy-current sensors to detect grinding burn marks on 42CrMo4 workpiece have been simulated. The impedance of the µCoils with varying geometries (i.e. circular non-spiral µCoil, circular spiral µCoil and meander type µCoil) changed in response to the presence of grinding burn mark, thereby aiding in their detection. The impedance response of the circular non-spiral and meander type µCoil is found to be almost similar. While the impedance response of circular spiral µCoil was better than the other two geometries, however from the microfabrication point of view its fabrication is complex. Therefore, the circular non-spiral µCoil was modified by increasing the width of non-circular spiral coil in a linear manner, whereby, the sensitivity and the strength of the impedance difference of µCoil in response to the grinding burn mark (for both 200 µm width and 1500 µm width grinding burn marks) is significantly improved. Furthermore, as proof of concept circular non-spiral µCoils with 5, 10 and 15 turns were fabricated using ferromagnetic nickel-cobalt alloys. The experimental results show that the impedance of the fabricated µCoil change in response to the grinding burn mark on 42CrMo4, thereby, confirming the feasibility of the application of µCoils for detection of grinding burn marks. Owing to their miniaturized size, these sensors can be embedded in the grinding tool for the real time in-situ monitoring of the grinding burn marks and other material flaws and also for the detection of grinding burn marks in µm dimensions.

Acknowledgement

The authors would like to thank the "Ministerium für Wissenschaft, Forschung und Kunst Baden-Württemberg"and "Europäische Fonds für regionale Entwicklung (EFRE)" for funding this research in the framework of the project "SensoGrind"(FEIH_KMU_1100458).

6. References/Literatura

[1] P.E. Mix, Introduction to nondestructive testing: A training guide, 2nd ed., Wiley, Hoboken N.J., 2005.
[2] Y. Hamasaki, T. Ide, Fabrication of multi-layer eddy current micro sensors for non-destructive inspection of small diameter pipes, in: Proceedings IEEE Micro Electro Mechanical Systems. 1995, IEEE, 29 Jan.-2 Feb. 1995, 232.
[3] D.J. Sadler, S. Gupta, C.H. Ahn, Micromachined spiral inductors using UV-LIGA techniques, IEEE Trans. Magn. 37 (2001) 2897–2899.
[4] D.J. Sadler, C.H. Ahn, On-chip eddy current sensor for proximity sensing and crack detection, Sensors and Actuators A: Physical 91 (2001) 340–345.
[5] M. Pan, Y. He, R. Xie, W. Zhou, The influence of MEMS on electromagnetic NDT, IEEE, 20.06.2014 - 23.06.2014, 363–367.
[6] H.H. Gatzen, E. Andreeva, H. Iswahjudi, Eddy-current microsensor based on thin-film technology, IEEE Trans. Magn. 38 (2002) 3368–3370.
[7] M.W. Seidel, A. Zösch, K. Härtel, Grinding burn inspection, Forsch Ingenieurwes 82 (2018) 253–259.
[8] Antje ZÖSCH, Christopher SEIDEL, Konstantin HÄRTEL, Martin Wolfgang SEIDEL Josef MAIER, Gerhard NEUN, Detection of Near Surface Damages in Crank Shafts by Using Eddy Current Testing, 19th World Conference on Non-Destructive Testing 2016.
[9] M.K. Sinha, D. Setti, S. Ghosh, P. Venkateswara Rao, An investigation on surface burn during grinding of Inconel 718, Journal of Manufacturing Processes 21 (2016) 124–133.